Tiling Vertices and the Spacing Distribution of their Radial Projection

Tobias Jakobi

Fakultät für Mathematik, Universität Bielefeld
Universitätsstraße 25, D–33615 Bielefeld, Germany

Abstract

The Fourier-based diffraction approach is an established method to extract order and symmetry properties from a given point set. We want to investigate a different method for planar sets which works in direct space and relies on reduction of the point set information to its angular component relative to a chosen reference frame. The object of interest is the distribution of the spacings of these angular components, which can for instance be encoded as a density function on $\mathbb{R}_+$. In fact, this *radial projection* method is not entirely new, and the most natural choice of a point set, the integer lattice $\mathbb{Z}^2$, is already well understood.
We focus on the radial projection of aperiodic point sets and study the relation between the resulting distribution and properties of the underlying tiling, like symmetry, order and the algebraic type of the inflation multiplier.

PACS: 45.30.+s, 61.44.Br

1 Radial Projection Method

Given a locally finite point set $\Lambda \subset \mathbb{R}^2$, the following procedure is applied (see Fig. 1 for an example):

(a) For a reference point $x_0 \in \Lambda$ determine the subset Λ' of points visible from this x_0. We call a point p *invisible* if there exists a $p_0 \in \Lambda$ such that

$$\exists\, t \in (0,1) \;:\; p_0 = x_0 + t \cdot (p - x_0)\;. \qquad (1)$$

(b) Select a radius $R > 0$ and project all $x \in \Lambda' \cap B_R(x_0)$ to $\partial B_R(x_0)$. If x is given as $(a,b) \in \mathbb{R}^2$, then this amounts to mapping x to $\arctan(b/a)$.

(c) The step in (b) produces a list of distinct (because of the visibility condition) angles $\Phi(R)$. Since Λ is locally finite, we can sort the list

$$\Phi(R) \;=\; \{\varphi_1, \ldots, \varphi_n\}$$

in ascending order. We also renormalise the φ_i with the factor $\frac{n}{2\pi}$, such that the mean distance between consecutive entries becomes 1.

(d) Define $d_i := \varphi_{i+1} - \varphi_i$ and consider the discrete probability measure

$$\nu_R \;:=\; \frac{1}{n-1} \sum_{i=1}^{n-1} \delta_{d_i}\;.$$

(e) Assuming that it exists, the spacing distribution is now obtained by taking the limit $R \to \infty$ in the sense of weak convergence of measures.

The choice of the point x_0 can be arbitrary and, in general the limit measure $\nu := \lim_{R\to\infty} \nu_R$ depends on it. For now, we restrict ourselves to reference points with *high symmetry* (see Fig. 2 and 3). Further investigations are needed to decide whether an averaging over multiple x_0 makes more sense here.

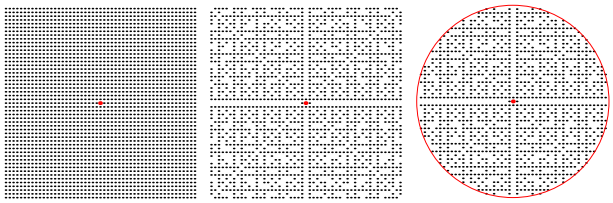

Figure 1: Radial projection using the example of the $\mathbb{Z}^2$ lattice.

All results (except for the reference cases) are currently strictly numerical and therefore rely on the computation of large circular patches of the point set and the determination of visibility. For an introduction to the topic of aperiodic tilings we refer to [1].

2 Integer Lattice $\mathbb{Z}^2$

The lattice $\mathbb{Z}^2$ provides the most ordered case of a planar point set. In this regard, it represents one reference point set for a potential classification of order. The set of visible points from the origin is given by

$$V_{\mathbb{Z}^2} \;=\; \{(a,b) \in \mathbb{Z}^2 \;:\; \gcd(a,b) = 1\}\;. \qquad (2)$$

*email: tjakobi@math.uni-bielefeld.de

In 2000, a closed expression [2] was derived for the limiting measure. With our setup, the explicit density function reads

$$g(t) = \begin{cases} 0, & 0 < t < \frac{3}{\pi^2}, \\ \frac{6}{\pi^2 t^2} \cdot \log \frac{\pi^2 t}{3}, & \frac{3}{\pi^2} < t < \frac{12}{\pi^2}, \\ \frac{12}{\pi^2 t^2} \cdot \log \left(2 \Big/ \left(1 + \sqrt{1 - \frac{12}{\pi^2 t}} \right) \right), & t > \frac{12}{\pi^2}, \end{cases}$$

but in fact the existence also holds for more general expanding regions (which is a circle here). A Taylor expansion of the tail of $g(t)$ gives

$$g(1/t) = \frac{36}{\pi^4} t^3 + \frac{162}{\pi^6} t^4 + \mathcal{O}(t^5) \quad \text{for} \quad t \to 0_+ \,, \qquad (3)$$

making it obvious that the moments of order $k \geq 2$ do not exist. A plot of $g(t)$ is overlayed over most histograms (see e.g. Fig. 4 and 5).
For all other cases (apart from the next), only histograms were computed.

3 Poisson Distributed Points

In contrast to the $\mathbb{Z}^2$ case, the point set generated by a homogeneous spatial Poisson process gives us the other reference point for our classification. In terms of order, it represents the case of total disorder. The model is also known as *complete spatial randomness* (CSR) or *ideal gas* in terms of physics.
Application of the radial projection procedure, with an arbitrary choice of reference point, yields a 1-dimensional CSR with intensity $\lambda = 1$ (due to the normalisation) in step (c). From there, it is not hard to see that the density of the radial projection measure is given by

$$f_\lambda(x) \;=\; \begin{cases} \lambda \exp(-\lambda x), & x \geq 0, \\ 0, & x < 0, \end{cases}$$

since step (d) just asks the question what the distribution of the waiting time between jumps of the process is.
The density $f_\lambda(x)$ (a plot can be seen in Fig. 9) therefore provides the second explicit function we can test histograms against.

4 Cyclotomic Model Sets and Visibility

Many aperiodic tilings can not only be realised by inflation of a set of prototiles, but by projecting a higher-dimensional lattice into $\mathbb{R}^2$. This is often described as the *cut and project* method or *model set* description.
Our general interest is in *cyclotomic* model sets, since these can be used to construct n-fold symmetric tilings. Also, this description is more suitable for radial projection since it only gives the tiling vertices and allows precise control over the patch size.
The Ammann–Beenker (AB) and the Tübingen triangle (TT) tiling can both be described as a cyclotomic

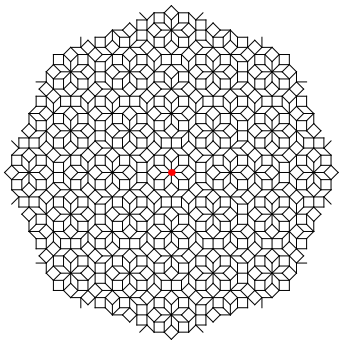

Figure 2: AB patch generated via projection.

model set (CMS) and the tiling vertices (the tiling in Fig. 2 uses the triangle/rhombus version) are given by

$$T_{\mathsf{AB}} = \{x \in \mathbb{Z}[\zeta_8] \;:\; x^\star \in W_8\},$$
$$T_{\mathsf{TT}} = \{x \in \mathbb{Z}[\zeta_5] \;:\; x^\star \in W_{10} + \epsilon\},$$

where the window W_8 is a regular octagon with edge length 1 centered at the origin.

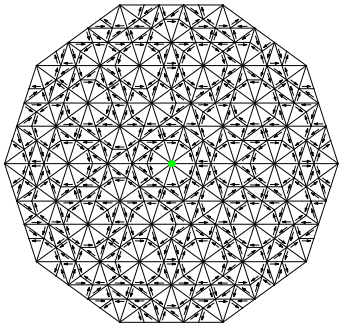

Figure 3: TT patch generated via inflation.

For the TT tiling the window W_{10} is a decagon, here with edge length $\sqrt{(\tau+2)/5}$ (τ denoting the golden mean). For the orientations of the windows, see Fig. 6. The map $\star$ is given by the extension of $\zeta_8 \mapsto \zeta_8^3$ in the AB case, and $\zeta_5 \mapsto \zeta_5^2$ in the TT one ($\zeta_n = \exp(2\pi i/n)$).

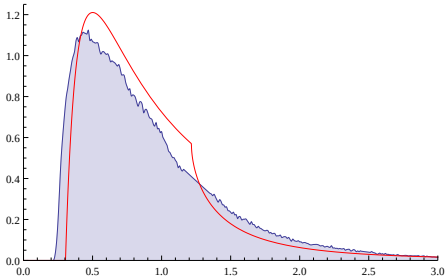

Figure 4: Spacing distribution of a large AB patch.

Another aspect of choosing this description is that the visibility test in Eq.(1) is computationally expensive compared to the local test (2) of the $\mathbb{Z}^2$ case. It turns out that a CMS also admits a similar description. For example, the visible points of the AB tiling with the reference point at the origin are

$$V_{\mathsf{AB}} = \{x \in T_{\mathsf{AB}} \;:\; \lambda_{\mathrm{sm}} x^\star \notin W_8 \text{ and } x \text{ is coprime}\},$$

with $\lambda_{\text{sm}} = 1 + \sqrt{2}$, the silver mean. The $\mathbb{Z}$-module in this case can be decomposed into $\mathbb{Z}[\zeta_8] = \mathbb{Z}[\sqrt{2}] \oplus \mathbb{Z}[\sqrt{2}] \cdot \zeta_8$ and coprime in this context means that for $\mathbb{Z}[\zeta_8] \ni x = x_1 + x_2 \cdot \zeta_8$ the $\gcd(x_1, x_2)$ is a unit in $\mathbb{Z}[\sqrt{2}]$.

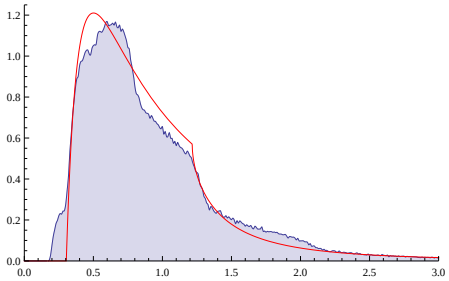

Figure 5: Spacing distribution of a large TT patch.

The same description can be given for the TT tiling and reads

$$V_{\mathsf{TT}} \;=\; \{x \in T_{\mathsf{TT}} \;:\; \tau x^\star \notin W_{10} + \epsilon \text{ and } x \text{ is coprime}\}\;,$$

with ϵ a small shift. Coprimality is defined as in the AB case, except that the module is $\mathbb{Z}[\tau]$ this time. The simplicity of these local visibility tests also depends on the order of

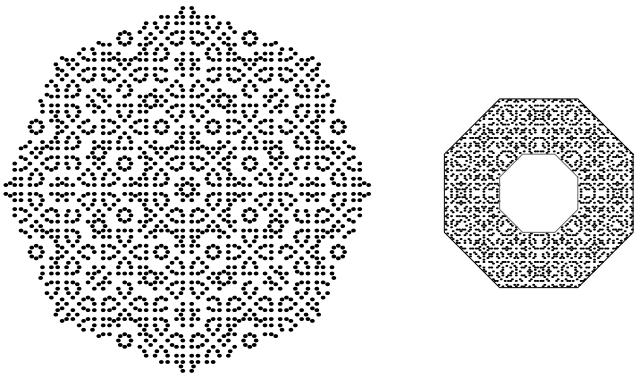

Figure 6: Visible vertices of the 8-fold AB tiling (left: direct space, right: internal space).

the underlying cyclotomic field, here a prime power.

5 A 12-fold Cyclotomic Case

Another tiling that is given by a CMS is the *Gähler shield* (GS) tiling. The vertices are

$$T_{\mathsf{GS}} \;=\; \{x \in \mathbb{Z}[\zeta_{12}] \;:\; x^\star \in W_{12} + \epsilon\}\;,$$

with a dodecagon W_{12} (edge length 1) and the map $\star$ given by the extension of $\zeta_{12} \mapsto \zeta_{12}^5$. The order of the cyclotomic field leads to a slightly more involved local visibility test

$$\begin{aligned} V_{\mathsf{GS}} \;= &\{x \in T_{\mathsf{GS}} \;:\; n(x) = 1 \wedge \lambda_1 x^\star \notin W_{12} + \epsilon\} \cup \\ &\{x \in T_{\mathsf{GS}} \;:\; n(x) = 2 \wedge \lambda_2 x^\star \notin W_{12} - \epsilon\}\;. \end{aligned}$$

The function n decomposes a $x \in \mathbb{Z}[\zeta_{12}]$ into the direct-sum representation

$$\mathbb{Z}[\sqrt{3}] \oplus \mathbb{Z}[\sqrt{3}] \cdot \zeta_{12} \quad \text{with} \quad \lambda_{12} := 2 + \sqrt{3}$$

and then computes $|N(\gcd(x_1, x_2))|$, the absolute value of the algebraic norm of the gcd of the components. The two *rescaling factors* for the visibility test are given by

$$\lambda_1 := \sqrt{\lambda_{12} \cdot 2} \quad \text{and} \quad \lambda_2 := \sqrt{\lambda_{12}/2}\;.$$

The first part of the set V_{GS} (indicated in **grey** in Fig. 7) comprises the already known coprime elements.

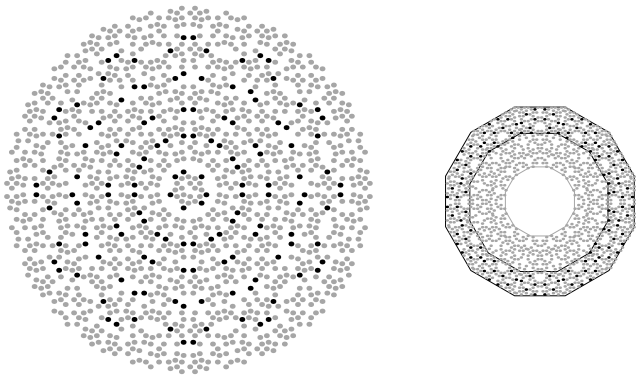

Figure 7: Visible points of a 12-fold GS tiling (left: direct space, right: internal space)

The **second part** is exceptional, and its existence is linked to the order 12 being a composite number.

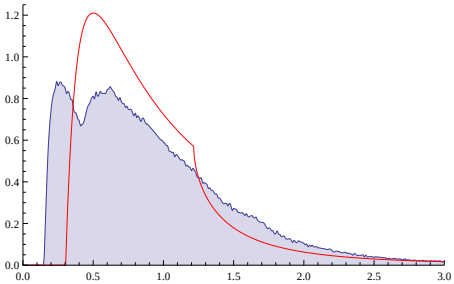

Figure 8: Spacing distribution of a large GS patch.

Even though Fig. 8 deviates a lot more from the $\mathbb{Z}^2$ distribution (compared to Fig. 4 and 5), all considered cyclotomic cases exhibit the special threefold structure (gap, bulk and tail). Let us consider a different tiling

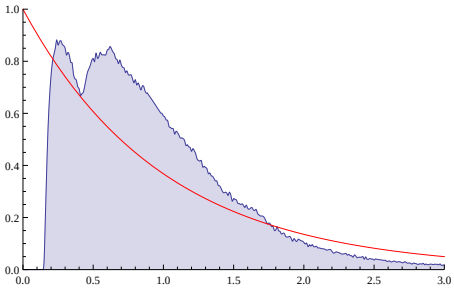

Figure 9: GS spacing distribution compared against Poisson.

with stronger spatial fluctuations.

6 A Non-Pisot Case / Lançon–Billard

The Lançon-Billard (LB) tiling is an example of a *chiral* (the tiles only appear in one chirality) inflation tiling with

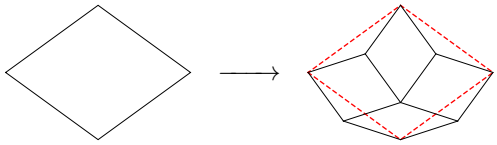

Figure 10: Tile A maps to 3×A and 1×B.

a multiplier $\lambda_{\mathsf{LB}} = \sqrt{(5+\sqrt{5})/2}$, which is a non-Pisot number. The inflation rules (a *stone* inflation is only

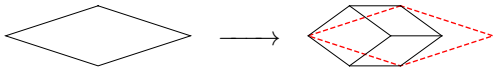

Figure 11: Tile B maps to 1×A and 2×B.

possible with a fractal tile boundary) generate a very irregular tiling.

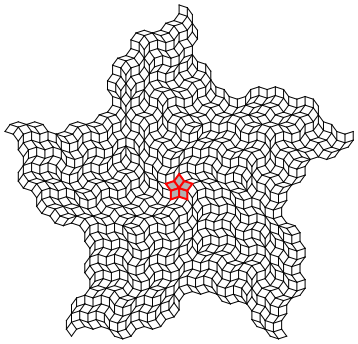

Figure 12: LB 5-fold symmetric patch.

The resulting distribution shows that the radial projection is sensitive to this irregularity.

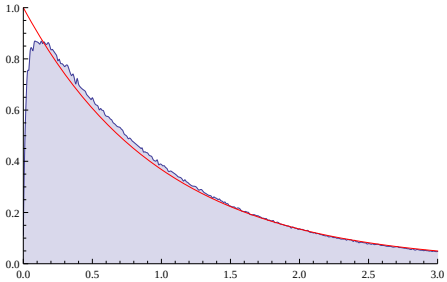

Figure 13: Spacing distribution of a large LB patch.

In fact, on this level, the LB tiling is almost indistinguishable from the Poisson case.

7 Some Additional Examples

We have already seen in Secs. 4 and 5 that the radial projection reacts to the order of symmetry of the tiling. The vertices of the *chair* tiling in Fig. 14 are a subset of

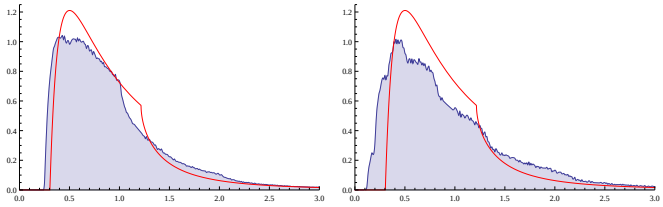

Figure 14: Spacing distribution of the *chair* (left) and *rhombic Penrose* (right) tiling.

$\mathbb{Z}^2$, but a different type of visibility condition has to be applied. The bulk section notices these changes, and

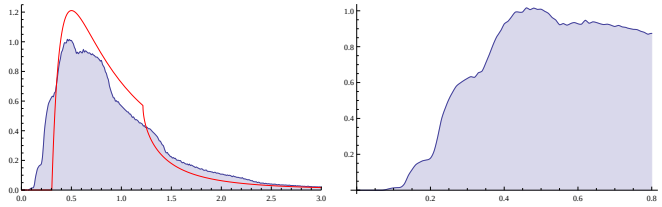

Figure 15: Spacing distribution of the *Penrose-Robinson* tiling and zoom into the bulk.

shows a lot of structure in general.

8 Tail Decay Behaviour

The expansion in Eq. (3) gives us an idea how the tail decay of the distribution behaves. A power law fit (c_k the coefficient of t^k) applied to the numerical data

tiling	gap size	c_3	c_4	e
$\mathbb{Z}^2$	0.304	0.369	0.168	—
AB	0.222	0.248	0.496	2.79
TT	0.182	0.239	0.513	2.60
GS	0.152	0.232	0.547	4.75

Table 1: Statistical data generated from the radial projection (e = error $\cdot 10^{-10}$).

indicates that at least the CMS cases also show a similar kind of decay.

Acknowledgement

The author wishes to thank Michael Baake, Markus Moll and Christian Huck for helpful discussions. This work is supported by the German Research Foundation (DFG) via the Collaborative Research Centre (CRC 701) at the faculty of Mathematics, University of Bielefeld.

References

[1] M. Baake and U. Grimm (2013). *Aperiodic Order Vol. I: A Mathematical Invitation.* (Cambridge University Press, Cambridge) (2013).

[2] F. P. Boca, C. Cobeli and A. Zaharescu, Distribution of lattice points visible from the origin. in: *Commun. Math. Phys.* **213**, 433–470 (2000).